Biradical formation by deprotonation in thiazole-derivatives: the hidden nature of Dasatinib

Carlos Heras,[1] Daniel Reta,[2*] Rosendo Valero[3,4] Guillem Albareda,[4,5] Nicholas F. Chilton,[2] Alistair J. Fielding,[5] Ibério de P. R. Moreira,[3,4*] Josep Maria Bofill,[1,4] and Francisco López-Calahorra,[1]

[1]Departament de Química Inorgànica i Orgànica, Sec. de Química Orgànica, Universitat de Barcelona, C/ Martí i Franquès 1, E-08028 Barcelona, Spain.
[2]School of Chemistry, The University of Manchester, Oxford Road, Manchester, M13 9PL, United Kingdom.
[3]Departament de Ciència dels Materials i Química Física, Sec. de Química Física, Universitat de Barcelona, C/ Martí i Franquès 1, E-08028 Barcelona, Spain.
[4]Institut de Química Teòrica i Computacional (IQTCUB), Universitat de Barcelona, C/ Martí i Franquès 1, E-08028 Barcelona, Spain.
[5]Max Planck Institute for the Structure and Dynamics of Matter and Center for Free-Electron Laser Science, Luruper Chaussee 149, 22761 Hamburg, Germany
[6]School of Pharmacy and Biomolecular Sciences, Liverpool John Moores University, Byrom Street, Liverpool, L3 3AF, United Kingdom.

Abstract

The formation of stable organic biradicals by a deprotonation process is reported for a series of conjugated heterocycles that share a Ph-N(H)-2-thiazole structural motif. We characterise the paramagnetic electronic ground state by means of continuous-wave and pulse EPR. We propose a simple valence bond mechanism for a deprotonation-induced formation of paramagnetic organic molecules, based on the interplay between the electronegativity of heteroatomic groups and the recovery of aromaticity to stabilise the biradical species. The Ph-N(H)-2-thiazole motif is found in a variety of biologically active molecules, exemplified here with the anticancer drug Dasatinib, and our results suggest a radical-based mechanism for the protein kinase inhibition activity of the drug. The existence of this structure-property relationship for an elementary chemical motif suggests that biradical species may be more prevalent than previously thought and have an important role in bioorganic chemistry.

1. Introduction

Most organic molecules present an even number of electrons distributed over doubly occupied molecular orbitals, resulting in diamagnetic ground states. However, applications derived from introducing unpaired electrons and thus magnetism into organic molecules are relevant across various fields, such as redox-biology,[1] optical devices,[2] reaction mechanisms,[3] multifunctional materials,[4] or spintronics.[5] Following the discovery of Gomberg's triphenylmethyl radical[6] and of Thiele[7] and Tschitschibabin[8] diradicals, a route to preventing electron-pairing and stabilising paramagnetic electronic states in organic molecules was developed. These works showed that careful design of the molecular topology[9] can lead to an electronic structure with two unpaired electrons weakly interacting in two nearly-degenerate non-bonding molecular orbitals[10,11] - the relative stabilization of the resulting spin-triplet

(*diradical*) *vs* the spin-singlet (*quinoidal*) states is dictated by an aromaticity gain on the cyclic subunits that links the radical centres (Scheme 1a).[12,13]

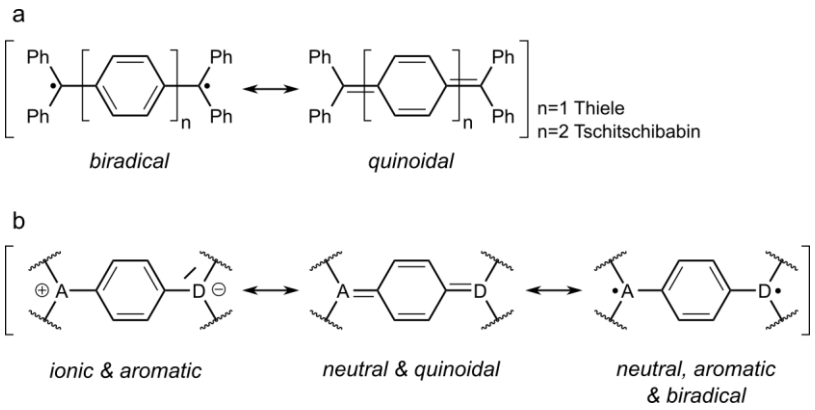

Scheme 1: Dominant valence bond forms in the electronic ground state of a) Thiele and Tschitschibabin hydrocarbons and b) heteroatom-containing (A, D) Thiele anion analogue. Unpaired electrons are indicated with dots.

EPR measurements show that in Tschitschibabin's[14-18] diradical, the energy separation between the ground spin-singlet and the excited spin-triplet states is thermally accessible ($\Delta E_{S-T} \sim 2.5\, Kcal/mol$) and MO calculations suggest the gap is 5.5 Kcalmol^{-1} in the Thiele hydrocarbon.[19,20]. Following these early works, this approach for designing stable organic radicals has been successfully applied to the general class of even alternant polyaromatic hydrocarbons (PAHs)[21] achieving almost degenerate spin states ($\Delta E_{S-T} \sim 0$), and more recently to analogues with unpaired electrons hosted on carbene-[22] and nitrogen-[23] centers, where ΔE_{S-T} can be modulated by varying the substituents – all these systems are symmetric, and to the best of our knowledge this approach has not been tested in asymmetric molecules. Importantly, these studies demonstrate that in principle, an appropriate linkage of adequate π-conjugated systems has the potential to yield organic molecules with diradical ground states. However, these systems contain only the most basic aspects that affect the molecular electronic structure, obviating multiple other features such as structural flexibility or the presence of multiple heteroatoms. Notably, heteroatoms can introduce ionic forms to accommodate unpaired electrons in otherwise inaccessible resonant paths, therefore offering promising, yet widely unexplored mechanisms to stabilize biradical states (Scheme 1b). In this simplified topological description, the two different heteroatoms (or heteroatomic groups, A and D) with different electronegativities, are connected via an aromatic bridging (ortho- or para-) ring that allows for their resonant interaction. The interplay between the groups A and D with the molecular charge offers resonant paths that are topologically equivalent (with a different charge distribution) to those obtained in Thiele's diradical, allowing for a redistribution of the electronic charge density on the molecule. In a first step, an anion is formed leading to a large electron density accumulated in D, which is alleviated by a charge transfer to the more electropositive A moiety, resulting in a neutral quinoidal form. Finally, the recovery of aromaticity drives the process toward the neutral aromatic diradical, which can be

further stabilised if the generated unpaired electrons can delocalise over the corresponding heteroatomic group. Thus, one might wonder whether more generic classes of molecules showing these extra degrees of freedom can also stabilise open-shell ground states.

In this work we set out to investigate this question and propose an alternative general approach to maximise the contributions that stabilise biradical ground states in organic molecules. In particular, we investigate a series of thiazole-based derivatives (Figure 1), as they are a general molecular class fulfilling the discussed topological arguments, have been investigated by some of us over the last years[24,25] and most importantly, present interesting reactivity profiles being used as anticancer[26-30] and antiviral[31,32] therapeutic agents. The herein proposed model has implications to understand the processes involved in the reactivity of these biologically relevant molecules, as exemplified by the results on **4**, the anticancer drug commercially known as Dasatinib (®Sprycel).

2. Results and discussion.

Compounds **1**-**4** (Figure 1) offer a set of molecules where the effects that contribute to the proposed biradical formation can be addressed separately, as they are introduced to varying degrees in each molecule. The synthesis and characterisation of compounds **1-3** is described in section 1 of the Supplementary Information (SI) - **4** was purchased, kept refrigerated and measured without any further manipulation. Common to all **1-4** is a structural consisting of *i)* an electron deficient aromatic group (NO_2 in **1**-**3**, amido group in **4**), *ii)* an electron donating aromatic group (thiazol group), and *iii)* a tautomeric enamine-imine linking group that results in amphoteric properties (1,4-phenylene in **1**, 2,6-acridine in **2** and **3**, and 2,4-thiazolyl in **4**). The amphoteric character of molecules **1**, **2** and **4** arises from the tautomerism of the imino-amino bridging group (also the amido group in **4**), whereas in molecule **3** it results from the acidity of the H atoms of the methyl group attached to the amine, that is largely increased by the adjacent positively charged nitrogen due to inductive and resonant effects. These are well-known effects[33] (Section SI 4 for details). In this case, this acidic proton can be exchanged between the methyl group and the imino-amino group bridging the thiazole and acridine moieties and is responsible of its amphoteric character.

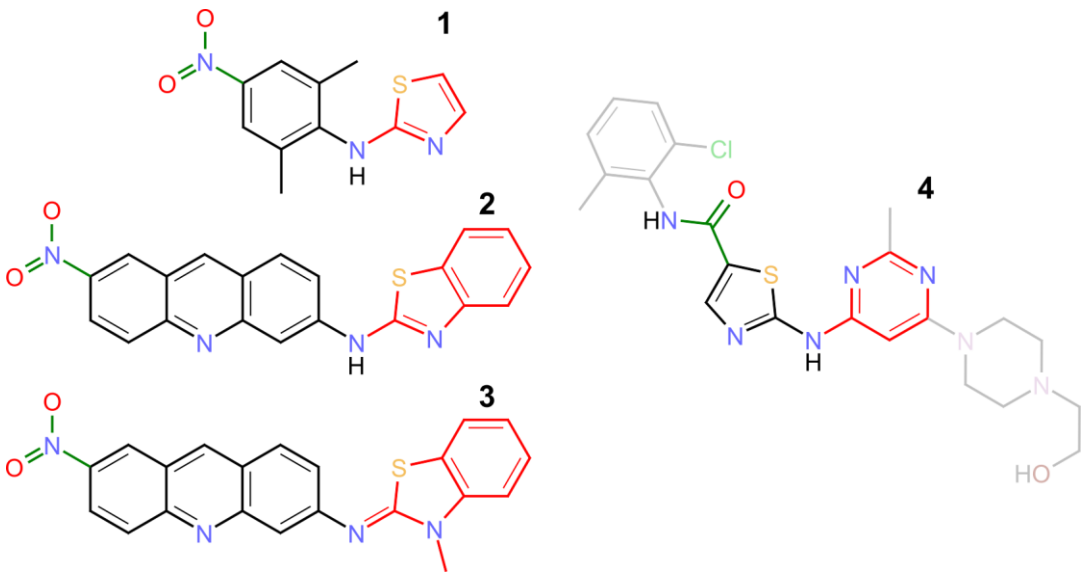

Figure 1: Schematic representation of **1-4**. Green, red and black bonds indicate electron deficient, electron donating and tautomeric linking groups (Scheme 1), respectively. **4** is known as Dasatinib.

To test whether the structural and electronic elements in **1-4** are effective at inducing biradical formation, we probe the electronic ground states of **1-4** via continuous-wave electron paramagnetic resonance (cw-EPR) spectroscopy, which selectively investigates the transitions associated with unpaired electrons. Variable temperature X-band (~ 9.4 GHz) EPR spectra were recorded for powder samples of all compounds (Figure 2, top row), showing a sharp isotropic transition centred at ~ 330 mT (g ~ 2), characteristic of organic radicals. The most intense signal (overall these are weak signals) is consistently obtained at the lowest temperature, and the signal reduces exponentially with increasing temperature; this is a typical feature arising from the Boltzmann population in a paramagnetic ground state. Molecules **2** and **3** show the most intense signals over the whole temperature range (based on signal-to-noise ratio), which we assign to a more effective delocalisation of the unpaired electrons over the extended conjugated π-system of acridine. Molecules **1** and **4** also show clear EPR transitions, but these are less intense due to the weaker electron withdrawing groups and the limited delocalisation over smaller π-systems. An EPR signal remains for **4** up to room temperature (Figure S5), but is omitted from Figure 2 for temperatures above 30 K for clarity.

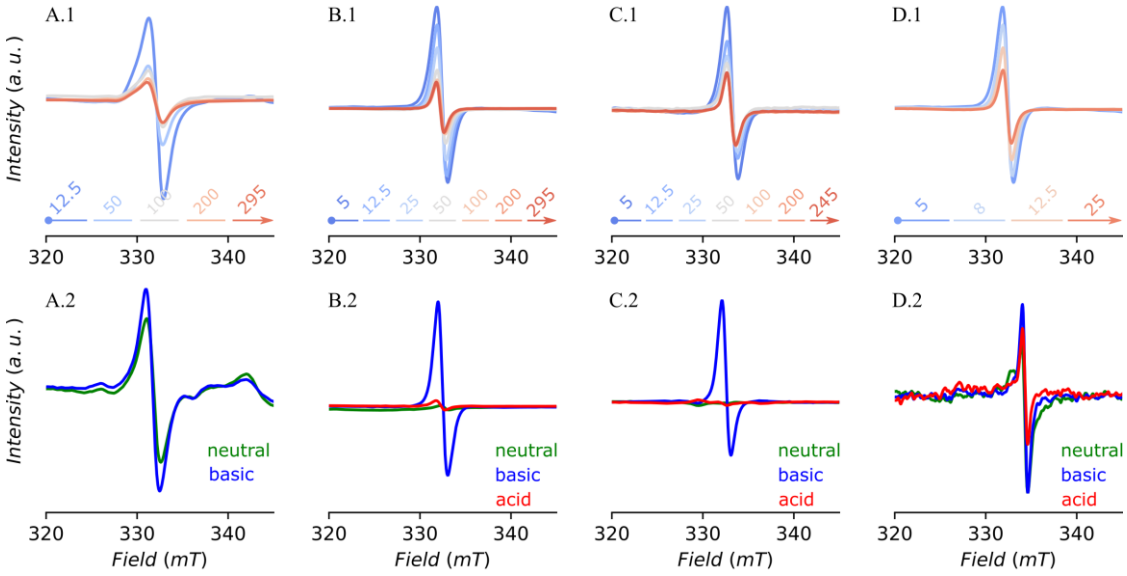

Figure 2: Normalised X-band EPR spectra for compounds **1-4**, A-D, respectively. Top row reports the temperature dependent powder spectra. Bottom row presents frozen solution spectra (12.5 K for **1**, 5 K for **2-4**) of the neutral, deprotonated and acidified samples.

Frozen solution X-band EPR measurements (Figure 2, bottom row and Figure S3) were performed to *i*) to probe the intramolecular origin of the observed signals in the powder measurements, and *ii*) to investigate the effect of deprotonation on the biradical character. Powder samples of **1** and **2-4** were dissolved in the aprotic solvents dichloromethane (DCM) and dimethylsulfoxide (DMSO), respectively, and degassed under a positive flow of He; all tubes were sealed with rubber caps to prevent contamination with paramagnetic molecular oxygen. An aprotic solvent is needed to avoid interference with the subsequent addition of a base to induce deprotonation. Frozen solution EPR spectra (labelled neutral in Figure 2) show signals at the same field position with comparable linewidths to the ones obtained in powder, confirming the intramolecular origin of the paramagnetic species. What appears to be fine structure in the frozen solution spectrum of **1** is the result of a weak signal after background-subtraction (see background in Fig S4). Molecule **3** also shows a very weak signal due to the small amount of sample that could be dissolved.

To probe the effect of deprotonation, approximately 50 μL of the strong base 1,8-diazabicyclo[5.4.0]undec-7-ene (DBU) was added to ~150 μL of neutral solution with a syringe through the rubber caps directly into the X-band tubes, under a positive flow of He. After mixing, the tubes were put back into the exact same position of the resonator. For all four samples, the colour of the solution drastically darkened on addition of base (Figure S24) and we observed a consistent increase in the EPR signal intensity (labelled basic in Figure 2) measured at the same temperature and position in the resonator.

Subsequent addition of acetic acid (labelled acid in Figure 2) reverts the process and results in either a reduction of the signal with respect to the basic solution (**4**), or its

almost entire suppression (**2-3**). For **1**, acid was not added because the last batch of that sample was left open to air and the signal decayed. In addition to the reduction of the EPR signal, the solution reverted to its original colour upon addition of acid (Figure S24).

To gain further insight on the effect of deprotonation and to connect the radical signals unambiguously to the structural motif in these molecules, we synthesised an analogue that shares the structural elements of **1-4** but lacks the acidic proton due to the absence of imine-enamine tautomerism. Figure 3 shows the X-band EPR silent spectra at 5 K of the powder and frozen DMSO solutions (6.55 mg dissolved in 200 µL of anhydrous DMSO), confirming that only the anionic form fulfils the topological conditions to host unpaired electrons, i.e., an acidic proton is crucial to stabilise a biradical configuration (see Figure S7 for more details). Note that the intensity scale is orders of magnitude smaller than for **1-4**, using a similar amount of sample.

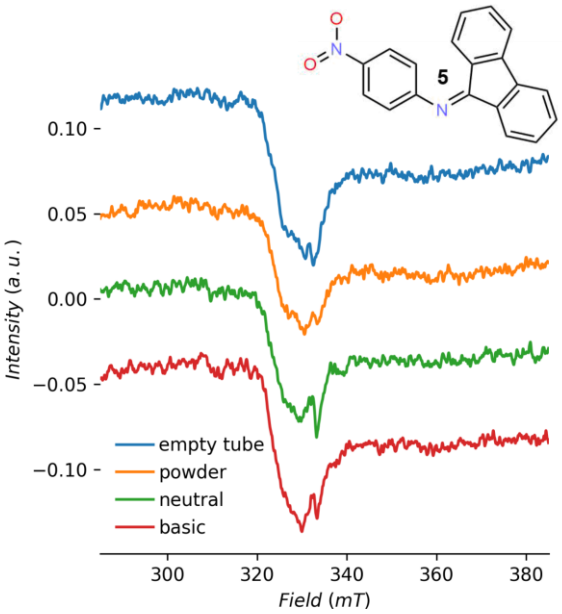

Figure 3: X-band EPR spectra of powder and frozen solutions of compound **5** at 5 K.

Having clarified that the anion is responsible for the paramagnetic response, it remains to determine if it is a mono- or biradical. The discrimination of these two situations is crucial since each one implies fundamentally different processes and mechanisms of formation, and has different properties. Unfortunately, the isotropic character of all EPR signals together with the absence of "half-field" or "forbidden" transitions (from the m_S = -1 to +1 of a possible biradical S = 1) can be explained assuming either a monoradical or a biradical with a very weak interaction between the two electrons, as indicated by our simulations (Section SI 2.1). The latter case has been observed before in bisgalvinoxyl,[34] where the EPR spectrum is characteristic of two independent doublets, and more recently in trioxotriangulene dimers,[35] where half-field transitions are not observed despite a confirmed triplet ground state. Thus here, we do not have the experimental evidence to say one way or the other, but we

can rationalise that these are biradicals with established chemical and reactivity arguments. We reason that if a mono-radical is created when the base is added, it must happen through a homolytic rupture of a labile bond in the molecule, leading to radical fragments that would rapidly react with other molecules – those could be identified in the final solution after neutralisation (e.g. by NMR), and would be different from the original solution. If instead a biradical is generated, the process could be reverted because no chemical bond needs to be broken. Figures S22-27 present the UV-Vis and NMR spectra of the neutral, basic and acidic solutions, showing that the pure and neutralised solutions are spectroscopically identical, whereas the intermediate basic solution shows distinctly different features. Finally, the possibility of an intermolecular biradical by an electron transfer in a pair of molecules is also not plausible, given the consistency of the results across molecules and solvents with different permittivity (**1** in DCM, **2-4** in DMSO). This, together with the increase in the EPR signal upon addition of base, confirms that the generation of the radicals is reversible and discards the possibility of a monoradical. Thus, a deprotonation-induced molecular biradical is the most consistent explanation of the observed paramagnetic response.

The measured data can be qualitatively explained using the topological and valence bond description presented in Scheme 2a. We discuss our model for **1**, but we theorise that it is a general mechanism applicable to any molecule containing the structural motif of Scheme 1b. Similar valence bond analysis for compounds **2-4** are in section 3 of the SI. Analogously to diamines or imidazole, the imine-enamine tautomerism of to the bridging nitrogen and the thiazole unit makes these molecules amphoteric, providing a mechanism for a fraction of the molecules to generate an anion from a proton transfer between two neutral molecules. In the solid state (powder measurements), the biradical species can be generated by a proton transfer between two identical amphoteric molecules during the formation of the solid as $2AH \leftrightarrow A^- + AH_2^+$ by precipitation from the solution. Thus, different precipitation methods mean different amounts of paramagnetic A^- being formed, as indicated by the magnetisation saturation values going from 84 to1.2 emu·mol^{-1} for **1** (Figure S19, measured on the same sample batch), depending on the precipitation method employed. In solution, the formation of the anion by this equilibrium is less favourable but still provides a defined fraction of deprotonated form at a given temperature - that fraction is largely increased in a basic medium (i.e. by adding DBU and ensuring an aprotic solvent). Additionally, the structural flexibility of the bridge allows for an out-of-plane conformation between the two aromatic groups, which could stabilise the biradical due to orthogonality of the magnetic orbitals.[36] Scheme 2a introduces the valence bond forms involved in the formation of the biradical **1** – among them, the one with the unpaired electrons on the bridging nitrogen and the NO_2 moiety is dominant due to a greater aromatic recovery (highlighted in blue square). Molecule **3** does not present an imine-enamine tautomerism and the formation of the anion involves the acidic methyl

hydrogens instead (section 4 of the SI). Nonetheless, the stabilisation of the biradical form is based on the same electronic processes as in the other molecules.

To obtain a better description of the biradical formation, we performed wave function and density functional theory calculations on **1**, as it is the simplest molecule (see Section S4 for details). However, all our approaches fail at predicting a consistent triplet-singlet gap, which is highly dependent on geometries, active spaces and basis sets; this speaks of the complexity of the problem, resulting from a critical combination of strong electronic correlation and electron-nuclear coupling effects. We suggest that the reversible deprotonation process induces a region of highly correlated electron-nuclear motion, allowing for a complex crossing of quasi-degenerate electronic states with different spin multiplicity (see Scheme 2b). Therefore, any attempt to describe this process cannot rely on the Born-Oppenheimer approximation of electron-nucleus separability, rendering any standard computational method inapplicable. Adding to this, one cannot include static electronic correlation in a balanced way for the two spin states (S_0 and T_0) with a reasonably sized active space due to the highly delocalized nature of the problem - as a result of this imbalance the singlet-spin state is artificially stabilized in our calculations. For instance, in similar compounds,[37,39] spin-polarisation arising from the σ-backbone needs to be treated as a first-order effect, making impractical any wavefunction-based approach to include further dynamic correlation or to construct a potential energy surface to perform a dynamics calculation.

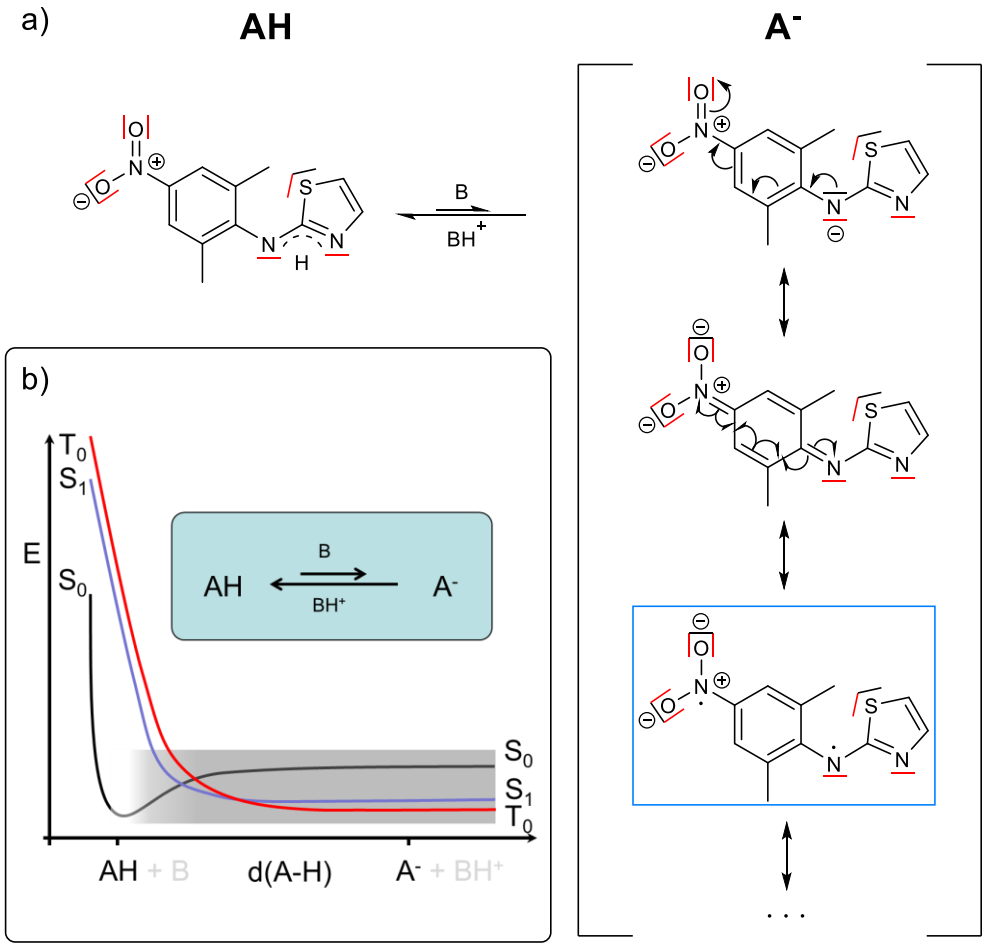

Scheme 2. a) Valence bond forms in the ground state of the anion of compound **1**. Unpaired electrons are represented by dots and the dominant biradical form is marked in blue. Red lone pairs cannot delocalise due to σ-π orthogonality. b) Model for the energy profile of the proton extraction process, responsible for the biradical formation. Darkened area indicates the region of strong electron-nucleus coupling and quasi-degenerate states with height of the order of k_BT.

In our proposed model, the unpaired electrons are mainly hosted by nitrogen and one would expect to observe hyperfine splitting due to the nuclear spin $I = 1$ of ^{14}N, in apparent contradiction with the measured cw-EPR data. However, considering the experimental EPR linewidth and hyperfine constants in line with literature values one can simulate an EPR spectrum with no hyperfine features (Figure S9). To gain further evidence towards the presence of ^{14}N hyperfine interaction and the validation of the model, pulse X-band experiments were performed for **2** and **3**; the signal for **4** is too weak to detect and we did not have more sample of **1**. Echo-detected field-swept (EDFS) spectra for **2** and **3** are presented in Figure S10-11, respectively. Compound **2** shows an intense transition at H_{dc} = 3550 G and a broad peak at H_{dc} = 3454 G, the latter being obscured in the cw-EPR. Collection of an EDFS spectrum at the same conditions of the empty resonator and empty tube confirm that this is not an artefact of the resonator. The derivative of the EDFS spectrum is consistent with that obtained from cw-EPR (Figure S12). The intense and broad transitions are assigned to each of the electrons in the biradical, one mainly localised on the bridging nitrogen and the

other delocalised over the acridine and nitro group (Figure S29). Conversely, compound **3** shows a single intense transition at H_{dc} = 3529 G, with no indication of the broad peak. In this case, the deprotonated methyl group participates of all resonant paths (Figure S30), resulting in a comparatively more delocalised unpaired electron which is not observed. For each maximum in the EDFS spectra of **2** and **3**, we performed 2- and 3-pulse X-band ESEEM experiments (Figure S13-16) to access the nuclear quadrupole interactions and obtain estimates of the nuclear ^{14}N hyperfine parameters; the advantage of a 3-pulse sequence is the absence of band combinations, which results in a cleaner spectrum. Figure 4 presents the frequency-domain 3-pulse ESEEM data for **3**, where the three nuclear quadrupole resonances and the double quantum transitions are identified, in line with reported values.[40-44] This provided a good starting point to fit the 3-pulse and simulate the 2-pulse data (Figure S17, see section 2.1.1 for details). In conclusion, we consistently observe the fingerprints of ^{14}N in **2** and **3**, which provides strong evidence towards the validity of the proposed model for the generation of the molecular biradical – this can be safely extrapolated to **1** and **4** due to the consistency of the different spectroscopic results.

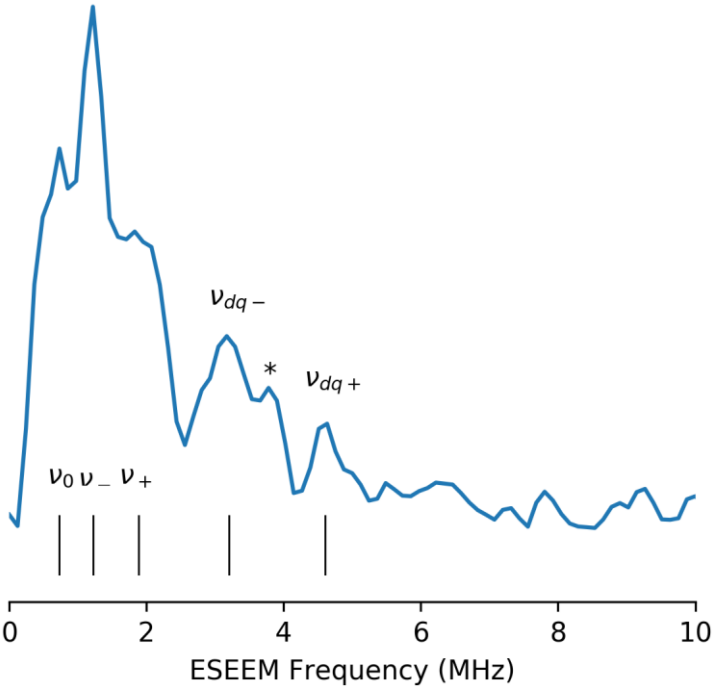

Figure 4. X-band frequency-domain of 3-pulse electron spin echo envelope modulation (ESEEM) for **3** at 5 K and 352.9 mT field position. * indicates the Larmor frequency ^{13}C.

The observed radical character of compound **4** (Dasatinib), deserves special attention. Dasatinib is an anticancer drug that binds to tyrosine kinase proteins and prevents cancer cells from multiplying.[45] It is used for treatment of Imatinib-resistant chronic myelogenous leukemia and is now being evaluated for use in advanced prostate and breast cancer.[46,47] Its mechanism of action is explained in terms of competitive interactions with the catalytic pocket or through allosteric interactions

with other regions of the kinase,[45] i.e. through electrostatic and dispersion forces. However, its anomalously high selectivity and efficiency could be better explained considering the formation of a local covalent bond via a radical-based mechanism. In fact, single crystal X-ray diffraction of the drug bound to the protein kinase[48] reveal that the bond distances of the C-N-C Dasatinib bridge are 1.37 Å, in between the distance expected for imine (C=N, 1.25 Å) and amine (N-C, 1.43 Å) bonds,[49] matching a conjugated $C \cdots N \cdots C$ bond as predicted by our model. Additionally, recent unexpected results on "exceptional cytotoxicities" of imido-ferrociphenols against triple-negative breast cancer (TNBC) cells have been correlated with the π system of their quinone methides constituents,[50] which interestingly share the same topological ingredients here discussed. Although speculative on its own, these observations become relevant in light of our EPR data.

3. Conclusions

We have characterised the molecular biradical nature of a series of thiazole-derivatives and assign the effect to a specific structural pattern. The biradical character is manifested in the anionic state of the molecules, further confirmed by EPR silent experiments on an analogue that does not possess an acidic proton. The unpaired electrons show interaction with the nuclear spin of ^{14}N, as determined by pulsed EPR on **2** and **3**. UV-Vis and NMR spectroscopy is employed to demonstrate that the protonation-deprotonation process is reversible, resulting in a stable biradical. We rationalise our findings based on a valence bond description of the available resonant forms in which the interplay between aromaticity of the bridging ring and molecular charge is key, and hypothesise that any molecule presenting the discussed structural motif should present a biradical character. The importance of this finding is exemplified by the results on Dasatinib (**4**), suggesting overlooked radical-based mechanisms for its biological activity. Altogether, our results call for a change of paradigm in the chemistry of thiazole-derived compounds.

Acknowledgments

This research was supported by the Spanish MINECO, the Agencia Estatal de Investigación (AEI), Fondo Europeo de Desarrollo Regional (FEDER; CTQ2016-76423-P), Spanish Structures of Excellence María de Maeztu program (MDM-2017–0767, Generalitat de Catalunya (grant 2017SGR348 and XRQTC), and the UK EPSRC (EP/P002560/1). G.A. acknowledges also financial support from the European Union's Horizon 2020 research and innovation programme under the Marie Skłodowska-Curie grant agreement No 752822. We thank the EPSRC National EPR Facility at The University of Manchester for EPR measurements, along with Prof. Eric McInnes, Prof. David Collison, Dr. Marie-Emmanuelle Boulon, Mr. Edmund Little and Mr. Adam Brookfield. We thank Alexis San Juan for NMR spectra.

References

[1] K. V. Avondt, E. Nur, S. Zeerleder, *Nature Reviews Nephrology*, 2019, **15**, 671 – 692.
[2] X. Ai, E. W. Evans, S. Dong, A. J. Gillett, H. Guo, Y. Chen, T. J. H. Hele, R. H. Friend, F. Li, *Nature*, 2018, **563**, 536–540.
[3] D. Leifert, A. Studer, *Angew. Chem., Int. Ed*. **2019**, doi.org/10.1002/anie.201903726.
[4] J. Veciana, I. Ratera, Chapter 2 in 2010, John Wiley & Sons, Ltd, ISBN:9780470666975.
[5] S. Sanvito, *Chem. Soc. Rev.*, 2011, **40**, 3336–3355.
[6] M. Gomberg, *J. Am. Chem. Soc.* 1900, **22** (11), 757−771.
[7] J. Thiele, H. Balhorn, *Ber. Dtsch. Chem. Ges.* 1904, **37**, 1463−1470.
[8] A. E. Tschitschibabin, *Ber. Dtsch. Chem. Ges.* 1907, **40**, 1810−1819.
[9] I. Gutman, O. E. Polansky, Springer-Verlag: New York, 1986.
[10] L. Salem, C. Rowland, *Angew. Chem., Int. Ed. Engl*. 1972, **11**, 92−111.
[11] M. Abe, *Chem. Rev.* 2013, **113**, 7011−7088.
[12]L. K. Montgomery, J. C. Huffman, E. A. Jurczak, M. P. Grendze, *J. Am. Chem. Soc.* 1986, **108**, 6004-6011.
[13] G. Trinquier, J. P. Malrieu, *Chem. Eur. J.*, 2015, **21**, 2, 814-828.
[14] C. A. Hutchison, A. Kowalsky, R. C. Pastor, G. W. Wheland, *J. Chem. Phys.* 1952, **20**, 1485.
[15] D. C. Reitz, S. I. Weissman, *J. Chem. Phys*. 1960, **33**, 700.
[16] R. K. Waring, G. J. Sloan, *J. Chem. Phys*. 1964, **40**, 772.
[17] H. M. McConnell, *J. Chem. Phys.* 1960, **33**, 1868.
[18] E. Muller, A. Rieker, K. Scheffler, A. Moosmayer, *Angew. Chem. internat. Edit.* 1966, **5**, 1.
[19] H. S. Jarrett, G. J. Sloan, W. R. Vaughan, *J. Chem. Phys*. 1956, **25**, 697.
[20] I. D. Morozova, M. E. Dyatkina, *Russ. Chem. Rev.* 1968, **37**, 376.
[21] Z. Zeng, X. Shi, C. Chi, J. T. Lopez Navarrete, J. Casado, J. Wu, *Chem. Soc. Rev.*, 2015, **44**, 6578—6596.
[22] D. Rottschäfer, N. K. T. Ho, B. Neumann, H. G. Stammler, M. van Gastel, D. M. Andrada, R. J. Ghadwal, *Angew. Chem. Int. Ed.* 2018, **57**, 5838 –5842
[23] G. Tan, X. Wang, *Acc. Chem. Res.* 2018, **50**, 1997-2006.
[24]A. Molinos-Gómez, X. Vidal, M. Maymó, D. Velasco, J. Martorell, F. López-Calahorra, *Tetrahedron* 2005, **61**, 9075 -9081.
[25]S. Latorre, I. de P. R. Moreira, B. Villacampa, L. Julià, D. Velasco, J. M. Bofill and F. López-Calahorra, *ChemPhysChem* 2010, **11**, 912-919.
[26] T. C. Mahesh, S. Patel, P. Modi, P. S. Brahmkshatriya, *Current Topics in Medicinal Chemistry*, 2016, **16**, 26, 2841 – 2862.
[27] M. D. Altıntop, B. Sever, B. A. Çiftçi, A. Özdemir, *Molecules*. 2018, **23**(6): 1318.
[28] A. Jamwal, A. Javed, V. Bhardwaj, *J. Pharm. BioSci.* 2013, **3**, 114-123.
[29] S. Jain, S. Pattnaik, K. Pathak, S. Kumar, D. Pathak, S. Jain, A. Vaidya, *Mini-Reviews in Medicinal Chemistry* 2018, **18**, 8, 640 – 655.
[30] T. Italo de Santana, M. Barbosa, P. A. T. de M. Gomes, A. C. N. da Cruz, T. Gonçalves da Silva, A. C. L. Leite, *European Journal of Medicinal Chemistry* 2018, **144**, 874-886.
[31] K. M. Dawood, T. M. A. Eldebss, H. S. A. El-Zahabi, M. H. Yousef, *European Journal of Medicinal Chemistry* 2015, **102**, 266-276.
[32] O. I. El-Sabbagh, M. M. Baraka, S. M. Ibrahim, C. Pannecouque, G. Andrei, R, Snoeck, J. Balzarini, A. A. Rashad, *European Journal* of *Medicinal Chemistry*, 2009, **44**, 9, 3746-3753.
[33] E. A. Anslyn, D. A. Dougherty, Modern Physical Organic Chemistry,University Science Books, Sausalito 2008 ISBN: 978-1-891389-31-3
[34] E. A. Chandross, *J. Am. Chem. Soc*. 1964, **86**, 1263.
[35] T. Murata, N. Asakura, S. Ukai, A. Ueda, Y. Kanzaki, K. Sato, T. Takui, Y. Morita, *ChemPlusChem* 2019, **84**, 1–7.

[36] L. Salem, John Wiley & Sons, Inc. New York, 1982, pp 90-91.
[37] N. Ferre, N. Guihery, J. P. Malrieu, *Phys. Chem. Chem. Phys.*, 2015, **17**, 14375—14382.
[38] J. P. Malrieu, R. Caballol, C. Calzado, C. J. de Graaf, N. Guihery, *Chem. Rev.* 2014, **114**, 429−492.
[39] G. Trinquier, J. P. Malrieu, *J. Phys. Chem. A* 2018, **122**, 6926−6933.
[40] S. R. Rabbani, D. T. Edmonds, P. Gosling, M. H. Palmer, *Journal of Magnetic Resonance* 1987, **72**, 2, 230-237.
[41] D. T. Edmonds, P. A. Speight, *Physics Letters A* 1971, **34**, 6, 325-326.
[42] A. T. Taguchi, P. J. O'Malley, C. A. Wraight, S. A. Dikanov, *J. Phys. Chem. B* 2014, **118**, 31, 9225-9237.
[43] J. McCracken, S. Pember, S. J. Benkovic, J. J. Villafranca, R. J. Miller, J. Peisach, *J. Am. Chem. Soc*. 1988, **110**, 1069-1074.
[44] C. E. Tait, P. Neuhaus, H. L. Anderson, C. R. Timmel, *J. Am. Chem. Soc.* 2015, **137**, 6670−6679.
[45] P. A. Jänne, N. Gray, J. Settleman, *Nature Reviews Drug Discovery*. 2009, **8** (9) 709–23.
[46] N. P. Shah, C. Tran, F. Y. Lee, P. Chen, D. Norris, C. L. Sawyers, *Science* 2004, **305**, 399−401.
[47] E. Weisberg, P. W. Manley, S. W. Cowan-Jacob, A. Hochhaus, J. D. Griffin, *Nat. Rev. Cancer* 2007, **7**, 345−356.
[48] J. S. Tokarski, et al. *Cancer Res*. 2006, **66**, 5790–5797. www.rcsb.org/structure/2GQG
[49] T. Ma et al., *Science*, 2018, **361**, 6397, 48-52.
[50] Y. Wang, P. Pigeon, S. Top, J. S. Garcia, C. Troufflard, I. Ciofini, M. J. McGlinchey, G. Jaouen, *Angew. Chem. Int. Ed.* 2019, **58**, 8421 –8425.